Capillary ordering and layering transitions in two-dimensional hard-rod fluids

Yuri Martínez-Ratón*
Grupo Interdisciplinar de Sistemas Complejos, Departamento de Matemáticas, Escuela Politécnica Superior, Universidad Carlos III de Madrid, Avenida de la Universidad 30, E–28911, Leganés, Madrid, SPAIN
(Dated: February 1, 2008)

In this article we calculate the surface phase diagram of a two-dimensional hard-rod fluid confined between two hard lines. In a first stage we study the semi-infinite system consisting of an isotropic fluid in contact with a single hard line. We have found complete wetting by the columnar phase at the wall-isotropic fluid interface. When the fluid is confined between two hard walls, capillary columnar ordering occurs via a first-order phase transition. For higher chemical potentials the system exhibits layering transitions even for very narrow slits (near the one-dimensional limit). The theoretical model used was a density-functional theory based on the Fundamental-Measure Functional applied to a fluid of hard rectangles in the restricted-orientation approximation (Zwanzig model). The results presented here can be checked experimentally in two-dimensional granular media made of rods, where vertical motions induced by an external source and excluded volume interactions between the grains allow the system to explore those stationary states which entropically maximize packing configurations. We claim that some of the surface phenomena found here can be present in two-dimensional granular-media fluids.

PACS numbers: 64.70.Md,61.30.Hn,61.20.Gy

I. INTRODUCTION

The effect of fluid confinement on phase transitions is nowadays an active line of scientific research due to the direct application of the theoretically predicted surface phase diagrams in the nanotechnology industry. Confining simple fluids, such as hard [1, 2] or Lennard-Jones [3] spheres, in a narrow slit geometry, results in a rich phase behavior, which has recently been studied in detail. Liquid crystals confined in nanopores is another typical example of systems with important applications in the industry of electronic devices. For this reason they have been extensively studied using theoretical models based on density-functional theory. In particular, capillary phase transitions exhibited by a nematic fluid confined between hard walls[4, 5], or walls favoring a particular anchoring [6], have been predicted. When non-uniform liquid-crystal phases, such as the smectic phase, are included in the study of confined systems, the resulting surface phase diagrams display a rich phenomenology, which includes wetting transitions, the appearance of smectic defects [7], and layering transitions [8].

The effect of confinement on two-dimensional fluids is also an interesting topic of research. Langmuir monolayers of lipids on the surface of water have been extensively studied in the last hundred years [9], and the discovery of structures and phase transitions in these systems has experienced a dramatic evolution driven by the new experimental techniques. Now it is possible to confine these two-dimensional systems by external potentials and study the influence of the confinement on the molecular packing of surface monolayers.

Another paradigm of two-dimensional systems where the confinement plays an important role is the packing structures formed by particles in granular media [10]. The crystallization of a quasi-two-dimensional one-component granular-disk fluid has recently been studied experimentally [11]. It was found that the properties of the crystal structure obtained (such as packing fraction, lattice structure, and Lindenman parameter) coincide with their counterparts obtained from MC simulations of a hard disk fluid. Recent experiments have found non-equilibrium steady states in a vibrated granular rod monolayer with tetratic, nematic and smectic correlations [12]. Some of these textures are similar to the equilibrium thermodynamic states of two-dimensional anisotropic fluids resulting from density-functional calculations [13] and MC simulations [14]. It was shown by several authors that the inherent states of some frozen granular systems can be described by equilibrium statistical mechanics [15]. Also, an experimental test of the thermodynamic approach to granular media has recently been carried out [16]. Confining two-dimensional granular rods in different geometries (circular, rectangular, etc.) results in spontaneous formation of patterns, with different orientationally ordered textures and defects next to the container [17]. The authors of Ref. [18] have carried out MC simulations of a confined hard disk fluid. They have found that the crystal phase fails to nucleate due to formation of smectic bands when the system is confined [18]. It would be interesting to device an experiment with confined granular disks with the aim of comparing the properties of the non-uniform stationary states with those obtained from the statistical mechanics applied to the hard disk fluid.

The main purpose of this article is the study of a confined two-dimensional hard-rod fluid. We are interested

*Electronic address: yuri@math.uc3m.es

in the calculation of the surface phase diagram of a hard rectangle (HR) fluid confined by a single or two hard lines. We can think on a HR fluid as an experimental realization of a system of hard cylinders confined between two plates at a distance less than twice the cylinder diameter. We suggest that some of the surface phase transitions obtained here by applying the density functional formalism to a confined two-dimensional HR fluid should be similar to the steady states of confined granular rods. Some experiments are required to verify this hypothesis.

The paper is organized as follows. In Sec. II we present the theoretical model: the fundamental-measure density functional applied to a HR fluid in the restricted-orientation approximation. This section is divided into two subsections. In the first the model is particularized to the study of the bulk phases, while in the second part the theoretical expressions used in the calculations of the thermodynamic and structural properties of the interfaces are presented. The results are presented in Sec. III. First we study the bulk phase diagram of a HR fluid with aspect ratio equal to 3, and then the resulting surface phase diagrams of a single wall-HR fluid interface and of the fluid confined between two hard lines are presented. Some conclusions are drawn in Sec. IV.

II. THEORETICAL MODEL

In this section we introduce the theoretical model used in the calculations of the bulk and interface equilibrium phases. To study highly inhomogeneous phases such as those resulting from the confinement of a fluid in a narrow slit geometry or the solid phase with a high packing fraction, we have used the Fundamental-Measure Theory (FMT) applied to an anisotropic fluid of hard rectangles. It is well known that this formalism presents a great advantage over other techniques when dealing with highly inhomogeneous phases, and that this is mainly due to the fact that a basic requirement to construct the FMT density functional is that it conform with the dimensional cross-over criterium [19, 20]. To implement the calculations we have used the restricted-orientation approximation, where the axes of the rectangles are restricted to align only along the coordinate axes x or y. Thus, the whole system is described in terms of density profiles $\rho_\nu(\mathbf{r})$ $(\nu = x, y)$.

While the ideal part of the free energy density in reduced thermal units has the exact form

$$\Phi_{\rm id}(\mathbf{r}) = \sum_\nu \rho_\nu(\mathbf{r}) \left[\ln \rho_\nu(\mathbf{r}) - 1\right], \tag{1}$$

the FMT interaction part of the 2D HR fluid is approximated [20] by

$$\Phi_{\rm exc}(\mathbf{r}) = -n_0(\mathbf{r}) \ln\left[1 - n_2(\mathbf{r})\right] + \frac{n_{1x}(\mathbf{r}) n_{1y}(\mathbf{r})}{1 - n_2(\mathbf{r})}, \tag{2}$$

where the weighted densities n_α's are calculated as

$$n_\alpha(\mathbf{r}) = \sum_{\nu=x,y} \left[\rho_\nu * \omega_\nu^{(\alpha)}\right](\mathbf{r}), \tag{3}$$

and where the symbol $*$ stands for convolution, i.e., $\rho_\nu * \omega_\nu^{(\alpha)} = \int_V d\mathbf{r}' \rho_\nu(\mathbf{r}') \omega_\nu^{(\alpha)}(\mathbf{r} - \mathbf{r}')$. The weights $\omega_\nu^{(\alpha)}$ are the characteristic functions whose volume integrals constitute the fundamental measures of a single particle (the edge lengths and surface area). They are defined as

$$\omega_\nu^{(0)}(\mathbf{r}) = \frac{1}{4}\delta(\frac{\sigma_\nu^x}{2} - |x|)\delta(\frac{\sigma_\nu^y}{2} - |y|), \tag{4}$$

$$\omega_\nu^{(1x)}(\mathbf{r}) = \frac{1}{2}\Theta(\frac{\sigma_\nu^x}{2} - |x|)\delta(\frac{\sigma_\nu^y}{2} - |y|), \tag{5}$$

$$\omega_\nu^{(1y)}(\mathbf{r}) = \frac{1}{2}\delta(\frac{\sigma_\nu^x}{2} - |x|)\Theta(\frac{\sigma_\nu^y}{2} - |y|), \tag{6}$$

$$\omega_\nu^{(2)}(\mathbf{r}) = \Theta(\frac{\sigma_\nu^x}{2} - |x|)\Theta(\frac{\sigma_\nu^y}{2} - |y|), \tag{7}$$

where $\sigma_\mu^\nu = \sigma + (L - \sigma)\delta_{\mu\nu}$, with L and σ the length and width of the rectangle and $\delta_{\mu\nu}$ the Kronecker function, while $\delta(x)$ and $\Theta(x)$ are the Dirac delta and Heaviside functions, respectively.

A. The bulk phases

To calculate the bulk phase diagram we need to minimize the Helmholtz free energy functional $\beta\mathcal{F}[\{\rho_\nu(\mathbf{r})\}] = \int d\mathbf{r}\left[\Phi_{\rm id}(\mathbf{r}) + \Phi_{\rm exc}(\mathbf{r})\right]$ with respect to the density profiles $\rho_\nu(\mathbf{r})$. These density profiles have the symmetries corresponding to the equilibrium phases, which can be the isotropic or nematic fluids, the smectic phase (with particles arranged in layers with their long axes pointing perpendicular to the layers), the columnar phase (with long axes parallel to the layers), plastic solid (particles located at the nodes of the square grid with averaged orientational order parameter over the cell equal to zero), and oriented solid (with both translational and orientational order). To take proper account of all these possible symmetries, we have used a Fourier-series expansion of the density profiles:

$$\rho_\nu(\mathbf{r}) = \rho_0 x_\nu \sum_{\mathbf{k}=(0,0)}^{\mathbf{N}} \alpha_{k_1,k_2}^{(\nu)} \cos(q_1 x)\cos(q_2 y), \tag{8}$$

where we defined $\mathbf{k} \equiv (k_1, k_2)$ [with $\mathbf{N} = N(1,1)$], $q_1 = 2\pi k_1/d_x$, and $q_2 = 2\pi k_2/d_y$ are the wave vector components parallel to x and y axes respectively, and d_x, d_y are the periods of the rectangular grid along these directions. $\alpha_{k_1,k_2}^{(\nu)}$ are the Fourier amplitudes of the density profile of the species ν with the constraint $\alpha_{0,0}^{(\nu)} = 1$. ρ_0 is the average of the local density over the cell, while x_ν is the cell-averaged occupancy probability of species ν. The Fourier series is truncated at that value N which guarantees that $\alpha_{N,N}^{(\nu)} < 10^{-7}$. With this parametrization the

weighted density can be calculated explicity as

$$n_\alpha(\mathbf{r}) = \rho_0 \sum_{\nu,\mathbf{k}} x_\nu \alpha^{(\nu)}_{k_1,k_2} \hat{\omega}^{(\alpha)}_\nu(\mathbf{k}) \cos(q_1 x)\cos(q_2 y), \quad (9)$$

where $\hat{\omega}^{(\alpha)}_\nu(\mathbf{k})$ are the Fourier transforms of the corresponding weights, which have the form

$$\hat{\omega}^{(0)}_\nu(\mathbf{k}) = \chi_0(q_1\sigma^x_\nu/2)\chi_0(q_2\sigma^y_\nu/2), \quad (10)$$
$$\hat{\omega}^{(1x)}_\nu(\mathbf{k}) = \sigma^x_\nu\chi_1(q_1\sigma^x_\nu/2)\chi_0(q_2\sigma^y_\nu/2), \quad (11)$$
$$\hat{\omega}^{(1y)}_\nu(\mathbf{k}) = \sigma^y_\nu\chi_0(q_1\sigma^x_\nu/2)\chi_1(q_2\sigma^y_\nu/2), \quad (12)$$
$$\hat{\omega}^{(2)}_\nu(\mathbf{k}) = a\chi_1(q_1\sigma^x_\nu/2)\chi_1(q_2\sigma^y_\nu/2), \quad (13)$$

Here $a = L\sigma$ is the surface area of the particle, and $\chi_0(x) = \cos x$, $\chi_1(x) = \sin(x)/x$. We have selected the orientational director parallel to y. Thus, the equilibrium smectic (columnar) phase should be found by minimizing the free energy with respect to the Fourier amplitudes $\alpha^{(\nu)}_{0,k}$ ($\alpha^{(\nu)}_{k,0}$), the smectic (columnar) period d_y (d_x) and the order parameter $Q_{\rm N} \in [-1,1]$ [related to the x_ν's through the relations $x_{\parallel,\perp} = (1 \pm Q_{\rm N})/2$ where the symbols $\parallel, \perp$ stand for particle alignment along y and x respectively]. For uniform phases [$\alpha^{(\nu)}_{k_1,k_2} = 0$ $\forall (k_1,k_2) \neq (0,0)$] $Q_{\rm N}$ coincides with the nematic order parameter. The solid phase is to be found by minimizing the free energy with respect to all the Fourier amplitudes $\alpha^{(\nu)}_{k_1,k_2}$, the crystal periods d_x and d_y, and the order parameter $Q_{\rm N}$ in the case of an orientationally ordered solid. To measure the packing structure and the orientational order of the bulk phases we use the local density and the order parameter profiles, $\rho(\mathbf{r}) = \sum_\nu \rho_\nu(\mathbf{r})$, and $Q(\mathbf{r}) = [\rho_y(\mathbf{r}) - \rho_x(\mathbf{r})]/\rho(\mathbf{r})$ respectively.

B. The interfacial phases

As we want to study the hard wall-fluid interface or the HR fluid confined in a slit geometry, we have introduced the following external potential:

$$V_\nu(x) = \begin{cases} \infty, & x < \sigma^x_\nu/2 \\ 0, & x \geq \sigma^x_\nu/2, \end{cases} \quad (14)$$

for the semi-infinite system, and

$$V_\nu(x) = \begin{cases} \infty, & x < \sigma^x_\nu/2 \quad \text{and} \quad x > H - \sigma^x_\nu/2 \\ 0, & \sigma^x_\nu/2 \leq x \leq H - \sigma^x_\nu/2, \end{cases} \quad (15)$$

for the slit geometry, where H is the slit width, and the normal to the wall was selected in the x direction. Note that this external potential represents a hard line which excludes the center of mass of particles at distances less than their contact distances with the wall. In this sense we can say that the external potential favors parallel alignment at the wall. This is in contrast with the favored homeotropic alignment usually considered in several studies of three-dimensional liquid crystals confined by a single or two walls (in particular that of Ref. [8]).

The one-dimensional equilibrium density profiles $\rho_\nu(x)$ were found by minimizing the excess surface free energy per unit length

$$\gamma \equiv \int dx \left\{ \frac{\Phi(x)}{\beta} + P - \sum_\nu \rho_\nu(x)\left[\mu_\nu - V_\nu(x)\right] \right\}, \quad (16)$$

where $\beta = (k_B T)^{-1}$, $\Phi(x) = \Phi_{\rm id}(x) + \Phi_{\rm exc}(x)$, and μ_ν are the chemical potentials of species ν fixed at the bulk fluid-phase value at infinite distance from the wall, while P is the fluid pressure. The chemical potential of the bulk fluid phase is calculated, as usual, as $\mu = \sum_\nu x_\nu \mu_\nu$, with x_ν the molar fractions of species ν. If the bulk phase is an isotropic fluid then $x_\nu = 1/2$, and $\mu_\nu = \mu$, $\forall \nu$.

To measure the degree of interfacial order, we will use the adsorption of the density profile, defined as $\Gamma = \int dx\,[\rho(x) - \rho(\infty)]$, and the order parameter profile $Q(x)$.

The expression (16) coincides with the definition of the surface tension of the wall-fluid interface for the semi-infinite case, which is approximately equal to half the excess surface free-energy for the slit geometry when the wall distance H is large enough to accommodate both interfaces.

To minimize the functional given by (16), we have discretized space in the x direction and minimize γ with respect to $\rho_\nu(x_i)$ ($x_i \in [x_0, x_N]$) using the conjugate-gradient algorithm.

III. RESULTS

In this section we present the main results obtained from the application of the theoretical model just described to the study of surface properties of a 2D HR fluid. Particles were chosen to have aspect ratio $\kappa \equiv L/\sigma = 3$. This aspect ratio is chosen because one of the aims of the present work is the study of layered phases confined by one or two walls. As we will show bellow for $\kappa = 3$ the stable phase is the columnar layered phase.

In the first subsection we will summarize the results obtained in the calculation of the bulk phase diagram of this system, while in the second subsection we will focus on the study of the surface phase diagram.

A. Bulk phase diagram

We have minimized the free energy density of the HR fluid, defined as $\Phi \equiv V^{-1}\int_V d\mathbf{r}\,[\Phi_{\rm id}(\mathbf{r}) + \Phi_{\rm exc}(\mathbf{r})]$, with respect to the Fourier amplitudes, periods, and mean occupancy probability, as described in detail in Sec. II A. The results are plotted in Fig. 1, where the free-energy densities of all the stable and metastable phases found are plotted as a function of the packing fraction $\eta = \rho_0 a$.

We have found, apart from the usual isotropic (I) and nematic (N) phases, two different smectic phases (Sm_1, and Sm_2), a plastic solid (PS), perfectly oriented solid (OS), and finally the columnar phase (C), which is the stable one in the whole range of packing fractions explored.

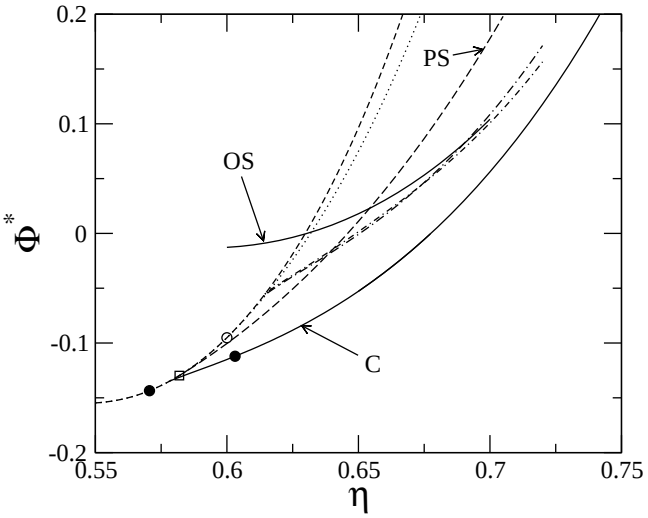

Figure 1: The rescaled free-energy density $\Phi^* = \Phi + 2.9875 - 5.8501\eta$ is plotted against the mean packing fraction for all the stable and metastable phases found. These are: isotropic (dashed line), nematic (dotted line), smectic-1 and smectic-2 (dotted and dashed lines), plastic solid (dashed line labelled as PS), while the perfectly oriented solid and the columnar phases (labelled in the figure as OS and C respectively) are plotted with solid lines. The open circle indicates the isotropic-nematic bifurcation point; the open square, the isotropic-plastic solid bifurcation point; and the solid circles represent the coexisting packing fractions at isotropic-columnar phase coexistence.

The coupling between the spatial and orientational degrees of freedom of the particles results in the presence of phases (stable or metastable) with different symmetries. In Fig. (2) we have sketched some of the particle configurations corresponding to phases with columnar (a), smectic-1 (b), smectic-2 (c), and plastic solid (d) symmetries found from the numerical minimization of the density functional. The directions of spatial periodicities of each phase have been depicted in the figure.

In Fig. 3 (a) we have plotted the density and order-parameter profiles of the coexisting columnar phase. The columnar phase is orientationally ordered in the y direction with the long rectangle axis pointing along the y axis, while the periodicity of both density and order parameter profiles (which are in phase) is along the x direction [see Fig. 3 (a)]. The mean coexistence packing fractions of the I and C phases are $\eta_{\rm I} = 0.57058$ and $\eta_{\rm C} = 0.60310$, respectively while the period of the C phase, in units of the HR width, was found to be $d_x/\sigma = 1.20102$. In Fig. 3 (b) we have plotted the order parameter $Q_{\rm N}$, and the period of the columnar phase as a function of the mean packing fraction.

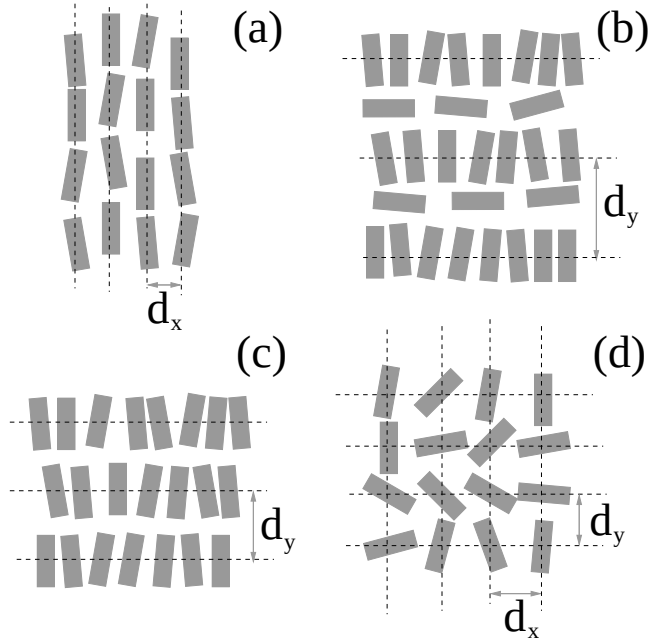

Figure 2: Sketch of particle configurations corresponding to different phases: columnar (a), smectic-1 (b), smectic-2 (c), and plastic solid (d) phases. The direction of spatial periodicities are labeled in the figure.

To compare the different packings of HR particles in the metastable phases (found as the local minima of the free energy density) for a fixed mean packing fraction $\eta = 0.7$, we have plotted the density and order-parameter profiles of the $Sm_{1,2}$ [Fig. 4 (a) and (b)], and PS and OS [Fig. 5 (a)–(c)] phases. As can be seen from Fig. 4 (a), the density profile of the Sm_1 phase has two maxima per period. The less pronounced maxima, located at the interstitials, reflect the high population of particles with long axes oriented parallel to the smectic layers [see the sketched particle configurations in Fig. 2 (b)]. This alignment is also shown in the order-parameter profile, which reaches high negative values at the interstitial positions. This phase bears a strong resemblance to the findings of Refs. [21] and [22] where the particle equilibrium configurations in the 3D smectic phases show the same pattern. As a consequence of this (alternating population of particles aligned perpendicular –sharpest peak in the density profile– and parallel to the layers), the smectic period in units of the particle length is $d_y/L = 1.53025$, higher than the smectic period of the Sm_2 phase ($d_y/L = 1.17935$). The density and order-parameter profiles of the Sm_2 are shown in Fig. 4 (b). As can be seen from the figure, these profiles reflect the usual packing in smectics, characterized by a single density peak with vanishingly small population of particles in the interstitials, while the order parameter reaches its maximum value at the position of the smectic layers [see Fig. 2 (c) for the sketched particle configurations].

The density and order parameter profiles of the PS phase with mean packing fraction equal to 0.7 are plot-

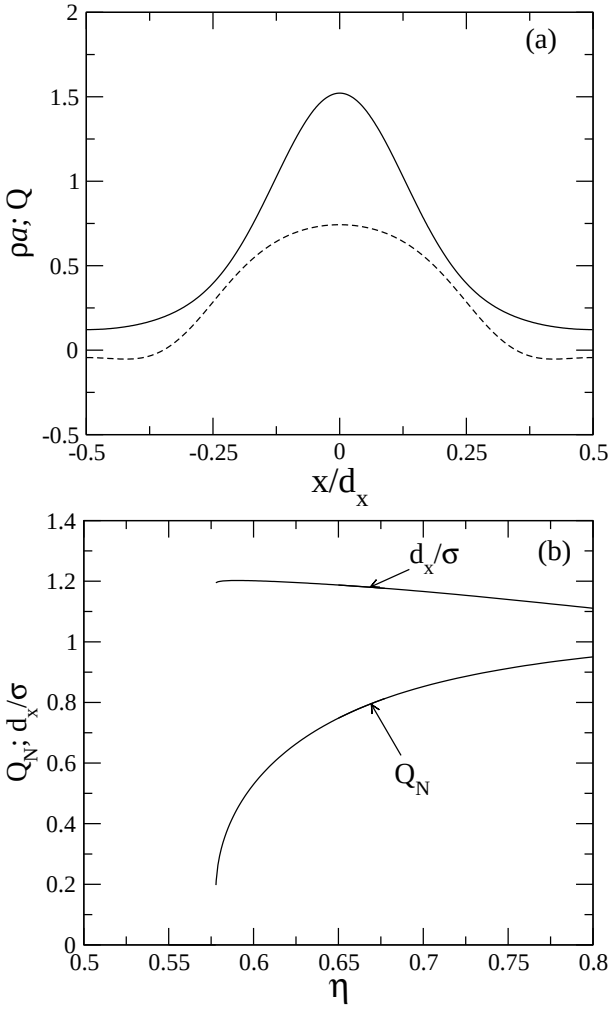

Figure 3: (a): density $\rho(x)$ (solid line) and order parameter $Q(x)$ (dashed line) profiles of the columnar phase at coexistence with the isotropic phase. (b): order parameter $Q_{\rm N}$ and period of the columnar phase against the mean packing fraction.

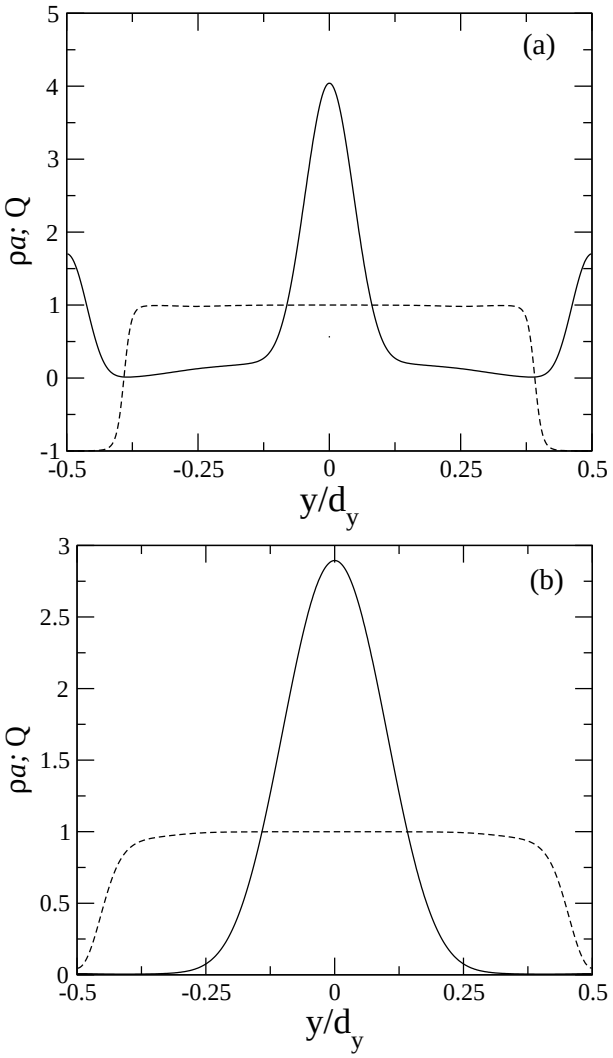

Figure 4: Density (solid line) and order parameter (dashed line) profiles of the smectic-1 (a) and smectic-2 (b) metastable phases for a value of mean packing fraction fixed at 0.7.

ted in Fig. 5 (a) and (b). The plastic solid has the same periodicity in the x and y direction, i.e. $d_x = d_y = d$, and the order parameter averaged over the unit cell is strictly equal to zero. As we can see from Fig. 5 (b), while the order parameter at the nodes of the square lattice is equal to zero, it reaches positive (negative) values at the $(\pm 0.5, 0)$ $[(0, \pm 0.5)]$ positions along the sides of the cell (the same solution with the x and y directions interchanged was found in the minimization of the free energy). Finally, the density profile of the perfectly aligned two-dimensional solid is plotted in Fig. 5 (c).

Although the phases described above are metastable with respect to the columnar phase, they can be stabilized for different values of the particle aspect ratio. A detailed study of the complete phase diagram, necessary to elucidate this point, is a work in progress.

We now proceed to make a comparison between the results for the 2D Zwanzig model with $\kappa = 3$ obtained above and those for hard parallelepipeds with restricted orientations and the same value of κ [23]. This comparison will show the differences in phase behaviour between three and two dimensions as predicted by Fundamental-Measure Theory (which, as already pointed out, conforms with the dimensional crossover criterion). As shown in Ref. [23], hard parallelepipeds exhibit a second-order phase transition between isotropic and plastic solid phases. As density increases the system goes to a discotic smectic phase (confirmed by simulations) via a first-order phase transition, which in turn discontinuously changes to a columnar phase and then to an oriented solid. By contrast, the present model shows that, in two dimensions, the isotropic phase exhibits a first-order transition to a columnar phase that is stable until very high packing fractions (more stable that plastic, oriented solid and different smectic phases). As a consequence, one expects that the corresponding surface phase diagrams be also

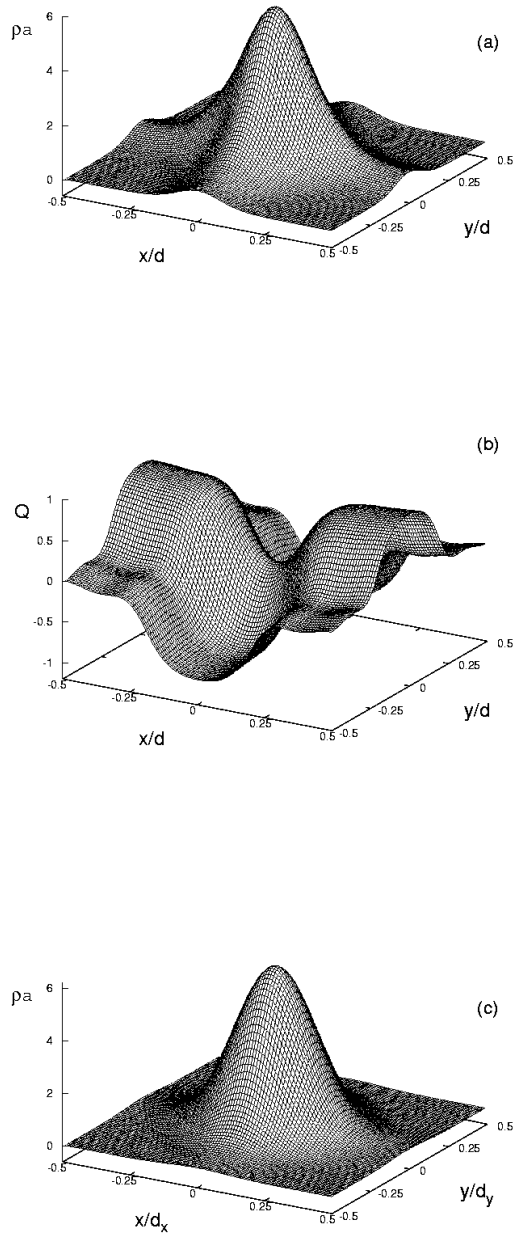

Figure 5: Density (a) and order-parameter (b) profiles of the plastic solid phase. (c): Density profile of the perfectly oriented solid.

different.

B. Surface phase diagram

In this section we deal with surface phenomena. In the first part we will concentrate on the semi-infinite wall-isotropic interface of a HR fluid, while in the second part we will focus on the slit geometry. We will demostrate the presence of complete wetting, capillary ordering and layering transitions in the confined two dimensional hard rod fluid. For a detailed discussion on general grounds of the phase behavior and critical phenomena of a confined by a single wall fluid see Ref. [24].

1. The wall-fluid interface

The interaction between the isotropic fluid phase and a hard wall was studied by calculating the one-dimensional equilibrium density $\rho(x)$ and order-parameter $Q(x)$ profiles through the excess surface free-energy minimization [see Eq. (16)]. The chemical potential μ of the fluid phase at infinite distance from the wall was varied within the range of isotropic-phase stability, i.e. $\mu \in [-\infty, \mu_0]$ (μ_0 being the value at which the I-C phase transition occurs). It is well known that the presence of a hard wall in a system of elongated particles induces parallel alignment of the particle axes with respect to the wall [25, 26]. This preferential alignment is a result of the entropic depletion effect. In the parallel configuration, the centers of mass of the particles are much closer to the wall, so the gain in volume per particle is larger and, as a consequence, the configurational entropy of the system is maximized. This effect is responsible for the occurrence of a biaxial nematic phase which breaks the orientational symmetry in a three-dimensional nematic fluid [4]. The same depletion mechanism is at work in 2D, as we will show below.

The results from the minimization are shown in Figs. 6 (a) and (b) for an undersaturation of $\beta\Delta\mu = -1.1\times10^{-4}$. As we can see from the figure, the density and order-parameter profiles indicate columnar order near the wall, which propagates several columnar periods into the fluid phase. The wall-fluid interaction enhances the orientational order near the surface and the adsorption of particles, creating a structured layer with columnar-phase symmetry which grows in width with increasing chemical potential and diverges at $\mu = \mu_0$. Thus, complete wetting by a columnar phase occurs at the wall-isotropic interface. This result is shown in Fig. 7 (a) where the excess surface free-energy γ and the adsorption coefficient Γ are plotted against $\Delta\mu = \mu - \mu_0$. As we can see, Γ grows continuously, ultimately diverging logarithmically with $\Delta\mu$ (see inset of figure). The excess surface free energy γ has a maximum, and at this point the adsorption passes through zero. This result is directly related to the interfacial Gibbs-Duhem equation, $\Gamma = -d\gamma/d\mu$, which relates the adsorption coefficient with the first derivative of the excess surface free-energy with respect to bulk chemical potential. At μ_0 the excess surface energy is equal to the wall-isotropic surface tension $\gamma_{\rm WI}$, which is in turn equal

to the sum of wall-columnar and columnar-isotropic surface tensions, $\gamma(\mu_0) = \gamma_{\rm WI} = \gamma_{\rm WC} + \gamma_{\rm CI}$ (the Young's equation for complete wetting).

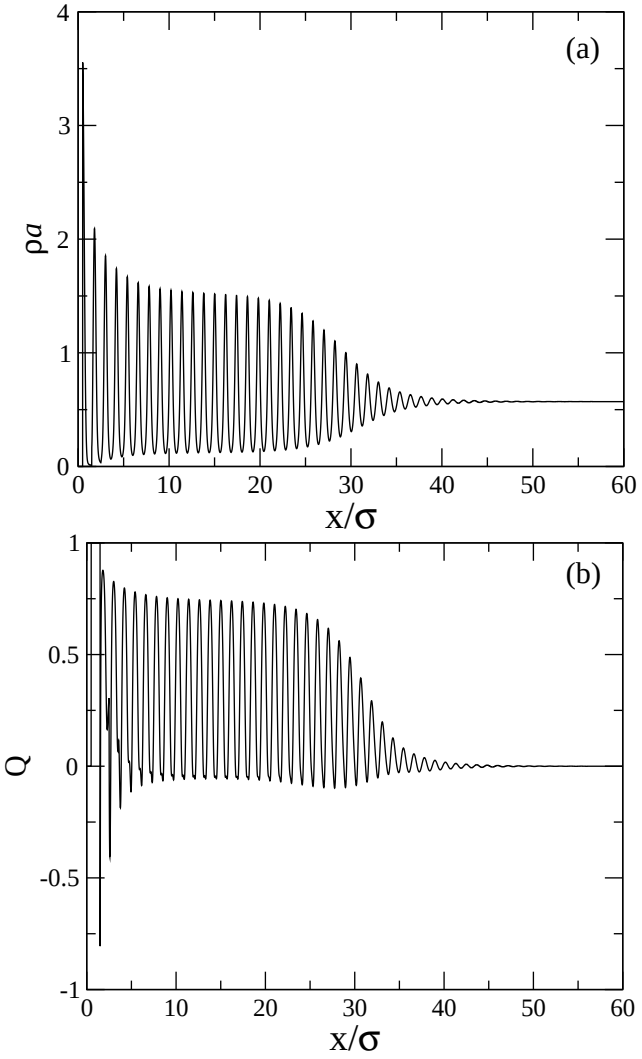

Figure 6: Density (a) and order parameter (b) profiles of the wall-isotropic fluid interface. The undersaturation is fixed to $\beta\Delta\mu = -1.1 \times 10^{-4}$.

We have carried out a logarithmic fit of the adsorption coefficient with respect to undersaturation $\beta\Delta\mu = \beta(\mu - \mu_0)$, and we find that $\Gamma\sigma = \tau_1 + \tau_2 \ln[\beta|\Delta\mu|]$, with $\tau_1 = 0.02387$ and $\tau_2 = -0.03396$. Then, integrating the interfacial Gibbs-Duhem relation $\Gamma = -d\gamma/d\mu$, we find the expression

$$\beta\gamma\sigma \approx \beta\gamma_{\rm WI}\sigma - [\tau_1 + \tau_2 (\ln(\beta|\Delta\mu|) - 1)]\,\beta\Delta\mu, \quad (17)$$

which approximates the excess surface free energy near complete wetting. The above expression is plotted against $\beta\Delta\mu$ in Fig. 7 (b), where the results from direct calculation of $\beta\gamma\sigma$, using the equilibrium density profiles obtained, are also plotted. As we can see the agreement is excellent even for relatively high values of undersaturation.

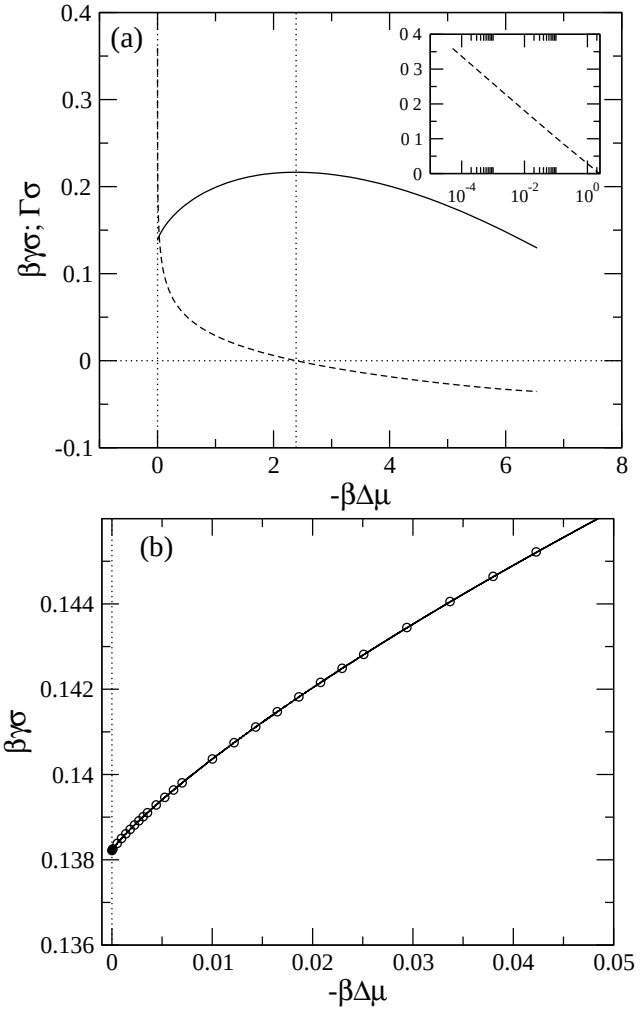

Figure 7: (a): excess surface free energy (solid line) and adsorption coefficient (dashed line), in reduced units, against $\beta\Delta\mu$. The inset shows $\Gamma\sigma$ vs. $\beta\Delta\mu$ in logarithmic scale. (b): excess surface free energy vs. $\beta\mu$ in the neighborhood of zero undersaturation. The open circles show the values obtained from the numerical minimization, while the solid line represents the analytic curve obtained by integrating the interfacial Gibbs-Duhem relation with the fitted logarithmic dependence of the adsorption coefficient (see text). The solid circle shows the value of the W-I surface tension $\beta\gamma_{\rm WI}\sigma = 0.13822$

To calculate the structural and thermodynamic properties of the columnar-isotropic interface, we have implemented a numerical scheme already used in Ref. [27], consisting of minimizing the surface excess free energy γ in a box of width h containing a stripe of a few columnar layers surrounded by isotropic material with periodic boundary conditions. h is chosen such that the density profiles can easily accommodate the two interfaces and go to the coexistence fluid density at the periodic boundary. A typical result from this calculation is plotted in Fig. 8 (a) and (b) for the density and order-parameter profiles, respectively. Thus, the I-C interfacial tension can be calculated as half the excess surface free energy

resulting from the minimization. We have found a value of $\beta\gamma_{\rm IC}\sigma = 0.00672$.

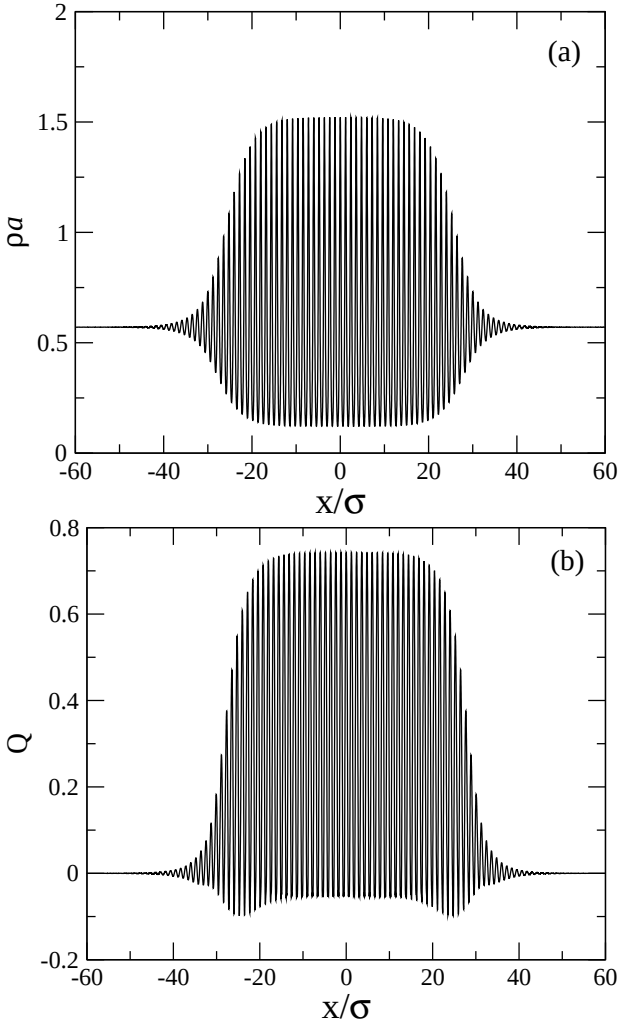

Figure 8: Density (a) and order-parameter (b) profiles of a numerical box containing two isotropic-columnar interfaces.

Finally, to verify that Young's law for complete wetting holds, we need to calculate the surface tension of the wall-columnar interface. To construct density profiles compatible with this semi-infinite interface, one has to establish a boundary, at the side of the computational box opposite to the wall, and place, beyond the boundary and into the bulk, a periodically structured profile, choosing the phase (i.e. the value of the profile at the boundary) arbitrarily within the bulk period. Although this recipe can in principle be implemented, we have chosen to fix bulk I-C coexistence conditions in a confined columnar phase and calculate the density profile of the system confined between two walls; the separation between the walls was chosen large enough so that the effects of having a finite interface penetration length caused by the presence of the confined external potential can be neglected. Also, in order to ensure that commensurability effects can be ignored, the distance between the walls was set to a (large) integer number of equilibrium periods of the columnar phase. The results from these calculations are plotted in Fig. 9 (a) and (b). The W-C surface tension calculated as half the value of the excess surface free energy results in $\beta\gamma_{\rm WC}\sigma = 0.13150$, compatible with Young's law in conditions of complete wetting of the W-I interface by the columnar phase.

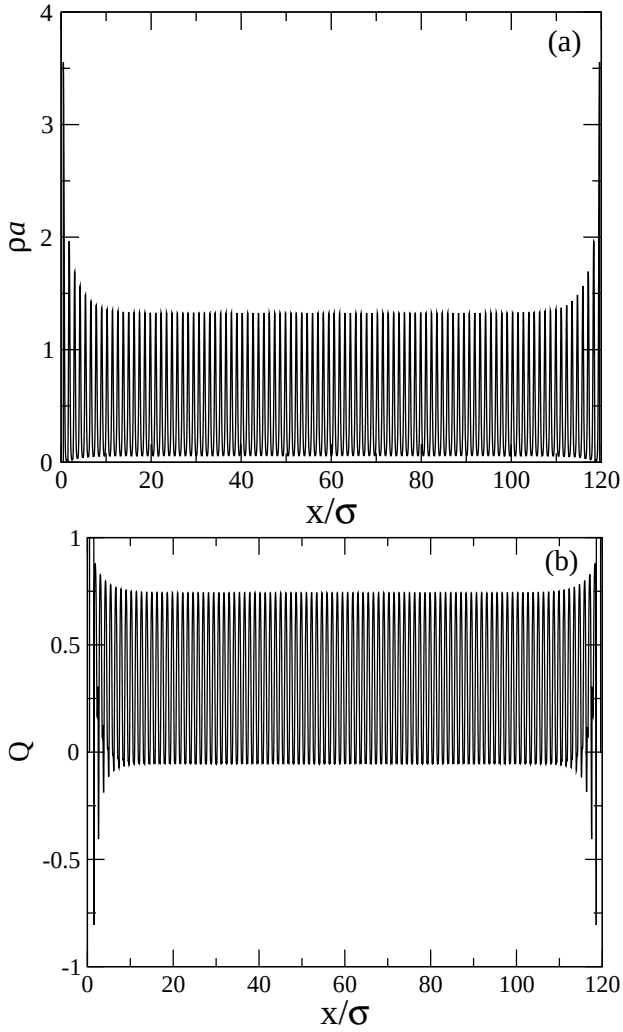

Figure 9: The density (a) and order parameter (b) profiles of two wall-columnar interfaces

2. Capillary ordering

This section is devoted to a study of the effect of confinement of a 2D HR fluid on the thermodynamic and structural properties of the fluid. In particular, we are interested in the enhancement of the orientational and layering ordering due to confinement, and the commensurability effects exhibited by a layered phase sandwiched between two hard walls at a distance that may or may not commensurate with the period of the bulk columnar phase. It is well known that, under certain circumstances

(related to the nature of the fluid-fluid and surface-fluid interactions), a fluid inside a pore can exhibit capillary first-order phase transitions between two different phases at a chemical potential below the bulk coexistence value. An example of this phenomenon is the recently studied capillary nematization [4] and smectization [8] of a liquid crystal fluid inside a pore. The bulk condensed phase may have uniform (nematic) or nonuniform density profiles. For the latter case, capillary layering transitions between interfacial phases with different number of smectic layers [8] can also be found. Here we will show that these capillary and layering phase transitions are not unique to 3D system. They are also present in 2D anisotropic fluids which can stabilize layered phases with different spatial symmetries, such as the columnar phase.

With a view to finding the effects of confinement on columnar ordering in a HR fluid, we have minimized the excess surface free energy with respect to the density profile for the particular case of HR's with $\kappa = 3$. The fluid is confined by two hard walls at a distance $H/\sigma = 30$ (in units of the particle width). As already pointed out, hard walls favor alignment parallel to the wall, as well as adsorption of particles at both surfaces (density and order parameters at contact are much higher than their bulk values). This coupled translational-orientational ordering near the surfaces propagates into the fluid, creating columnar ordering. We have found that for low values of the chemical potential of the bath the density profile is structureless (except just at the wall contact), similar to the bulk isotropic phase. Increasing the chemical potential several damped columnar peaks appear near the wall in a continuous fashion, i.e. with their heights increasing continuously. At some value of the chemical potential, the system exhibits a first-order phase transition between a phase with highly damped columnar peaks to a new phase with much stronger columnar ordering even at the center of the pore. The typical density and order-parameter profiles of both interfacial phases are shown in Fig. 10 (a)-(d). Although the less-ordered phase exhibits strong oscillations in both density and order-parameter profiles, the peak amplitudes are damped into the pore faster than those of the higher ordered phase. We will take the convention to call the first 'isotropic', and the second 'columnar' surface phases. This convention is justified by the fact that, just before the transition described above, columnar ordering increases continuously, starting from an isotropic-like density profile, as the chemical potential is increased. Thus we cannot trace out a definite boundary (a value for μ below that corresponding to first order phase transition) below or above which the profile inside the pore can be considered isotropic or columnar. Only the first order phase transition described above can really distinguish two different surface phases, one of them less ordered (following our convention, the isotropic phase) than the other (the columnar phase). As we can see in the figure, the latter has 25 columnar peaks.

The transition point is calculated from the discontinuity in the first derivative of the excess surface free energy with respect to the bulk packing fraction η. The corresponding plot is shown in Fig 11 (a). At this point the adsorption coefficient jumps discontinuously from the less- (the damped columnar) to the higher-ordered phase [see Fig. 11 (b)].

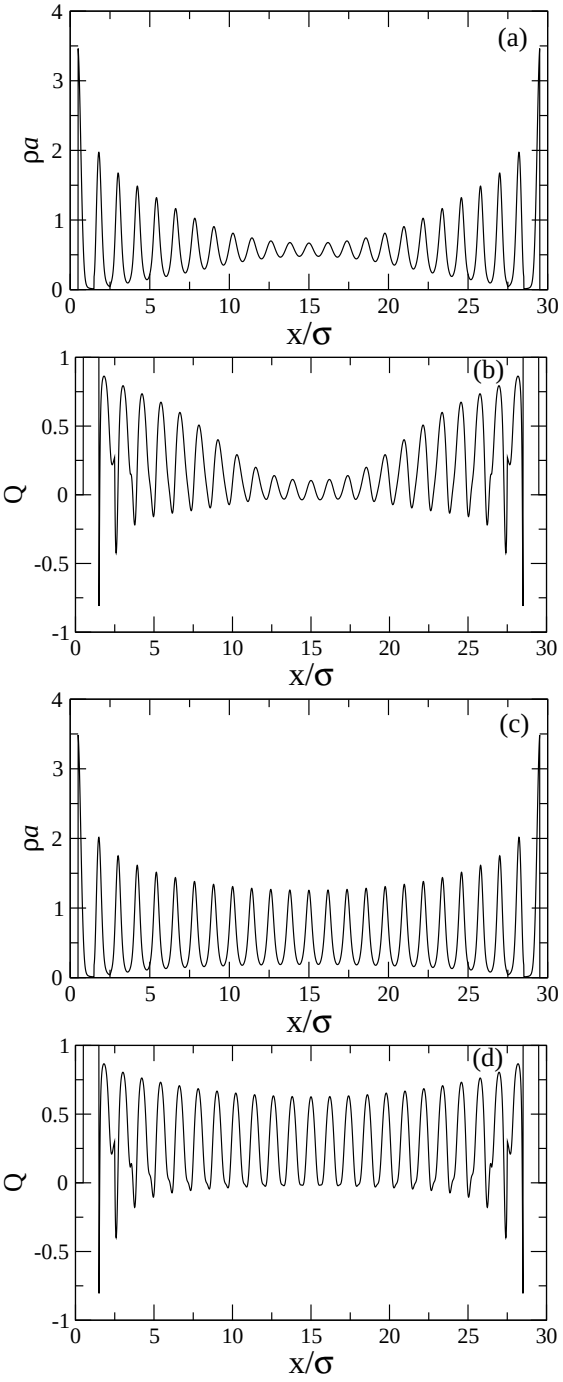

Figure 10: Isotropic (a)-(b) and columnar (c)-(d) phases that coexist at the same chemical potential bellow μ_0. (a), (c): Density profiles. (b), (d): Order-parameter profiles.

This surface transition point is located below the bulk isotropic-columnar phase transition [see Fig. 11 (a)],

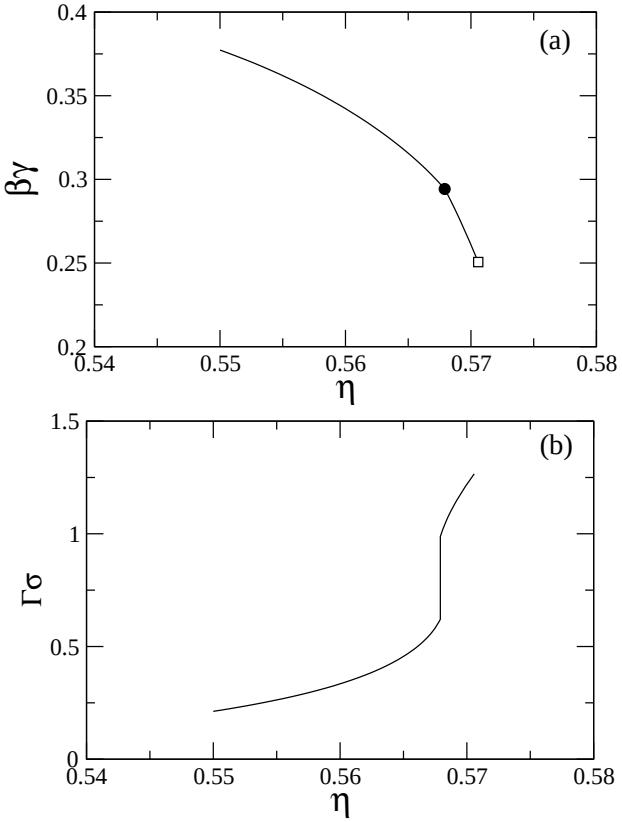

Figure 11: Excess surface free energy (a) and adsorption coefficient (b) against packing fraction of the bulk isotropic fluid. In the figure at top, the solid circle represents the transition point between both interfacial phases, while open square indicates the point corresponding to the bulk coexistence value for isotropic and columnar phases.

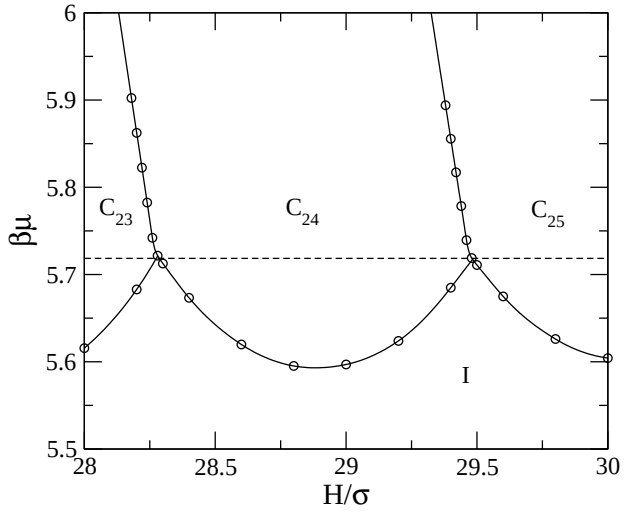

Figure 12: $\mu - H$ surface phase diagram showing first-order capillary columnar ordering and layering transitions. The pore width covers a range which goes from 23 to 25 columnar layers, as labeled in the figure. The open circles indicate the cases chosen for calculations, while the solid line is a cubic spline interpolation. The horizontal dashed line shows the value of the bulk chemical potential at the isotropic-columnar phase coexistence.

showing the presence of columnar-order enhancement in the pore. On further increasing the chemical potential up to a sufficiently high value (above μ_0), we find a first-order layering transition between two interfacial columnar phases which differ by just a single columnar layer. The behavior of the excess surface free energy and the adsorption coefficient is similar to that shown in Fig. 11 (a) and (b). Alternatively we can find the transition from $n-1$ to n columnar layers by fixing the chemical potential and increasing the pore width H.

The two surface phase transitions described above, namely first-order capillary I-C ordering and $(n-1)$–n layering transition, are connected in the $\mu - H$ surface phase diagram through the peculiar structure shown in Fig. 12.

The parabola below the bulk transition line corresponds to first-order transition lines separating regions of stability of the isotropic and the columnar interfacial phases, while the straight lines indicate layering transitions. Increasing the chemical potential from low values to those corresponding to the parabola, the density profiles always change continously from a structureless to damped columnar density profile. Both types of transitions (the isotropic-columnar and $n-1$-n layering transitions) coalesce in triple points, two of which are shown in Fig. 12. At the triple points an isotropic and two columnar interfacial phases with $n-1$ and n layers coexist in equilibrium. The set of connected of Fig. 12 are similar to those found in MC simulations of the confined hard-sphere fluid [2]. In this work the authors have shown the existence of capillary freezing of the HS fluid, confined in the slit geometry, for chemical potential values below the bulk freezing transition. The transitions lines in the $\mu - H$ surface phase diagram follow the same topology of connected set of parabolas as found in our system.

Some of the topological features of this surface phase diagram can be elucidated from the Clausius-Clapeyron equation as applied to the interfacial coexistence lines. The excess surface free energy $\gamma(\mu, H)$ along coexistence is a function of two variables, the chemical potential μ, and the pore width H. Thus, infinitesimal changes in these variables along the coexistence curve are related through the equation

$$d\gamma_\alpha - d\gamma_\beta = \Delta\left(\frac{\partial\gamma}{\partial\mu}\right)_H d\mu + \Delta\left(\frac{\partial\gamma}{\partial H}\right)_\mu dH = 0, \quad (18)$$

where the coexisting condition $\gamma_\alpha = \gamma_\beta$ (for α, β =I,C_{n-1},C_n) was used, and $\Delta u = u_\alpha - u_\beta$ for any function u. Using the interfacial Gibbs-Duhem equation $\partial\gamma/\partial\mu = -\Gamma$ and the definition of the solvation force $f = -\partial\gamma/\partial H$, we arrive at

$$\frac{d\mu}{dH} = -\frac{\Delta f}{\Delta\Gamma}, \quad (19)$$

which relates the first derivative of the chemical potential with respect to the pore width with changes in the solvation force and in the adsorption coefficient at the transition point. The negative slope of the layering curves is a direct result of Eq. (19), as the increment in the adsorption is always positive for the $(n-1) \to n$ layering transition, while the change in the solvation force is also positive (the latter can be interpreted as an increment with respect to the bulk of the excess surface pressure, which is obviously larger for the phase with n layers). For values of the pore width that commensurate with an integer number of columnar periods of the bulk columnar phase, the solvation force becomes zero and we get a minimum in the I-C capillary transition curve (see Fig. 12). At each side of the minimum the solvation force change the sign to positive (left side) or negative (right side) as we compress or expand the film, respectively, while the change in adsorption remains positive.

The Kelvin equation for capillary condensation in a slit geometry relates the undersaturation in chemical potential with pore width H as

$$\Delta\mu = \mu(H) - \mu_0 = -\frac{2\gamma_{\alpha\beta}}{(\rho_\alpha - \rho_\beta)H}, \qquad (20)$$

where ρ_α and ρ_β are the bulk coexisting densities of phases α and β (α being the condensed phase), while $\gamma_{\alpha\beta}$ is the surface tension of the corresponding interface. It was assumed that complete wetting by the α phase occurs at the W-β interface. For a detailed discussion of the Kelvin equation in the context of liquid crystal phase transitions see Ref. [28]. Applying this equation using $H/\sigma = 28.88$ (the location of the minimum in the $\mu - H$ phase diagram of Fig. 12), we obtain an undersaturation $\beta\Delta\mu = -0.0429$, while its real value is $\beta\Delta\mu = -0.1255$. In the derivation of the Kelvin equation, deviations from the bulk structure of the density profile arising from the confinement by the external potential are neglected. Also, the elastic energy resulting from the compression or expansion of a layered phase confined between two walls is not taken into account. These effects might be responsible for the differences found between our calculations and the estimation based on the Kelvin equation. We have checked that the sequence of minima in the $\mu - H$ phase diagram tends to μ_0 as $H \to \infty$, a result predicted by Eq. (20).

Refs. [4] and [8] showed that the capillary nematization line of the confined liquid-crystal fluid ends in a critical point for small values of the pore width. In order to study how the topology of the surface phase diagram changes in the regime of small pore widths, we have carried out the corresponding calculations of interfacial structure. We have found that the I-C capillary ordering transition changes at some particular value of H (near its maximum undersaturation represented by the minimum in the I-C interface coexisting curve) from first to second order. For lower values of H two critical points emerge from this single point, the distance between them increasing. In Fig. 13 one of these scenarios is shown. As we can see, there is a range of values of H (near the triple points) where the first-order capillary ordering transitions are still present but, between the critical points belonging to different layering branches, columnar ordering grows continously from the isotropic (damped columnar interfacial phase) to a highly-ordered columnar phase. Layering transitions are always present even for very small H, as will be shown below. An interesting feature of this phase diagram is that the location of the triple points moves above the bulk coexistence value μ_0. This indicates that the interfacial columnar phase just below the triple points can be unstable for values of chemical potentials corresponding to those of columnar-phase stability at bulk (similar to the capillary evaporation of the confined fluid). For wide enough slits (those for which the parabolas are connected) the triple points are practically located at μ_0, as can be observed from Fig. 12.

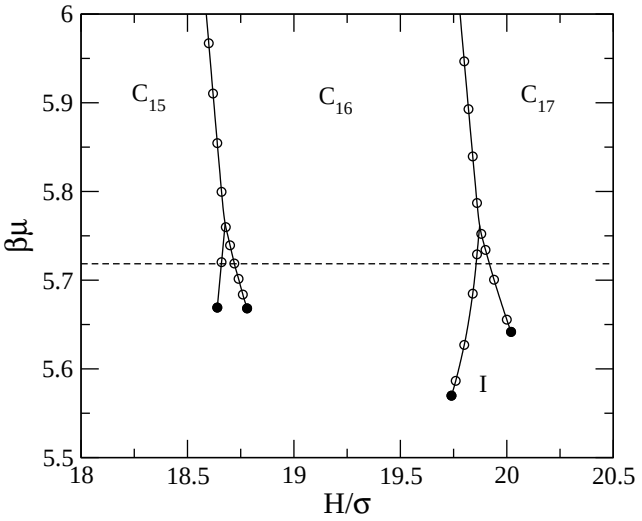

Figure 13: $\mu - H$ surface phase diagram showing critical points (filled circles). Number of columnar layers are indicated as subscripts.

For even smaller values of H, only layering transitions remain; these end in critical points located above μ_0, as Fig. 14 shows.

When the width H is such that the pore can only accommodate one particle with its long axis perpendicular to the wall (or not more than four or three particles aligned parallel to the wall) the system is near the one-dimensional limit. It is known that hard-core systems in this limit do not exhibit first-order phase transitions, but even for very narrow slits we can still find first-order transitions at which the density profile experiences an abrupt change inside the pore. In Fig. 15 (a) and (b) we show two coexisting density profiles corresponding to oversaturations, $\beta\Delta\mu = 0.51760$ and $\beta\Delta\mu = 0.72836$, and pore widths $H/\sigma = 4.32$ and $H/\sigma = 3.14$ in (a) and (b), respectively. The fluid inside the pore undergoes a phase transition, which dramatically changes the structure of the interfacial density profiles by increasing the heigh of

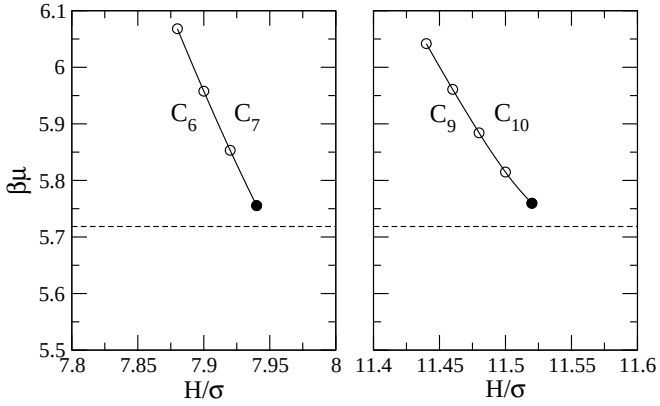

Figure 14: $\mu - H$ surface phase diagrams for small values of H.

four [Fig. 15(a)] or three [(b)] density peaks inside the pore.

IV. CONCLUSIONS

In this article we have shown that 2D fluids composed of anisotropic particles interacting via hard-core repulsion and confined in a slit geometry exhibit a complex and rich interfacial phase behavior. Apart from first-order capillary columnar ordering, we have also found layering transitions in this system. These results are similar to those found in 3D liquid-crystal fluids confined in a pore, where capillary smectization and layering phenomena were also found [8]. In view of these similarities, we can extract the conclusion that, independent of the system dimensionality and the peculiarities of the layered phases, either smectic or columnar, if the fluid-wall interaction enhances layered interface ordering (homeotropic in case of smectic phases, and the entropically favored parallel alignment for the columnar phase), compatible with the equilibrium bulk phase, then the confined fluid exhibits the interfacial phase transitions described above.

In this study we have used as a model a hard-rectangle fluid, and the density and the order-parameter profiles were calculated by minimizing the excess surface free-energy functional resulting from the Fundamental-Measure Theory applied to the two-dimensional Zwanzig model. The orientational degrees of freedom were discretized, in order to take advantage of having a free-energy functional which reduces to the exact one-dimensional functional when the density profile is constrained to lie along a line. This property is crucial to study strongly confined fluids (as is the case in this study), in particular when the pore width has only a few particle diameters in width.

As already pointed out in Sec. I, some experiments had shown profound similarities between particle configurations obtained as stationary states of systems of anisotropic grains and those corresponding to the equi-

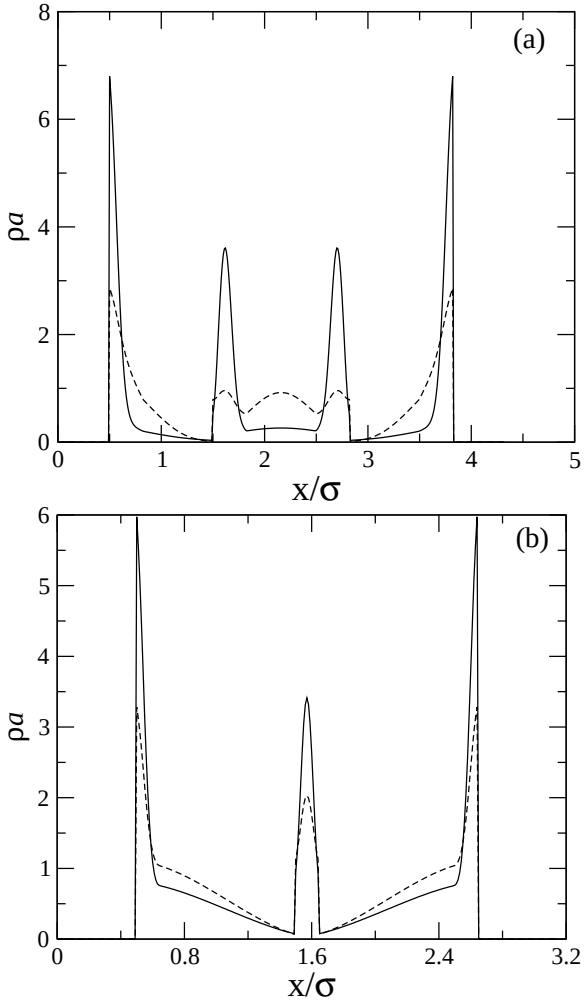

Figure 15: (a): density profiles of two coexisting phases (shown with solid and dashed lines) at $\beta\Delta\mu = 0.5176$. The pore width is $H/\sigma = 4.32$. (b): same as in (a) but for a pore with $H/\sigma = 3.14$ and for $\beta\Delta\mu = 0.72836$.

librium states obtained by density functional minimization [12]. These similarities can be explained by applying a maximum-entropy principle on granular collections of particles, i.e. for a fixed packing fraction, externally-induced vibrational motion forces the system to explore those stationary states which maximize the configurational entropy (since the grains cannot overlap). Of course, equilibrium statistical mechanics is unable to propose an equation of state for granular matter, but it could be possible to predict that granular matter composed of anisotropic particles and confined between parallel walls may support a stationary texture consisting of layers of particles oriented parallel to the wall. The manner in which the grain orientations propagate into the container would depend on the average packing fraction and on the frequency of the external force. Only at this qualitative level can we give some insight into possible complete wetting phenomena and capillary ordering in granular rod fluids confined between two horizontal plates at a

distance slightly larger than the particle dimensions in the vertical direction (thus simulating a two-dimensional system), and also confined by one or two vertical planes (these playing the role of hard walls).

Some calculations (not shown here) on the 2D HR fluid show that, for different aspect ratios, 2D smectic and crystal phases can be stable over some range of packing fractions. It would be interesting to explore whether confinement suppresses or enhances bulk ordering, and to study the changes in the surface phase diagram when phases of different symmetries are included. Work along this direction is currently in progress.

Acknowledgments

I thank D. de las Heras, E. Velasco, and L. Mederos for useful discussions, and E. Velasco for a critical reading of the manuscript. The author gratefully acknowledges financial support from Ministerio de Educación y Ciencia under grants No. BFM2003-0180 and from Comunidad Autónoma de Madrid (S-0505/ESP-0299) and (UC3M-FI-05-007). The author was supported by a Ramón y Cajal research contract from the Ministerio de Educación y Ciencia.

[1] M. Schmidt, and H. Löwen, Phys. Rev. Lett. **76**, 4552 (1996); Phys. Rev. E **55**, 7228 (1997).
[2] M. Dijkstra, Phys. Rev. Lett. **93**, 108303 (2004); A. Fortini, and M. Dijkstra, J. Phys. Condes Matter **18**, L371 (2006).
[3] L. Salamacha, A. Patrykiejew, S. Sokolowski, and K. Binder, Eur. Phys. J. E **13**, 261 (2004); L. Salamacha, A. Patrykiejew, S. Sokolowski, Eur. Phys. J. E **18**, 425 (2005).
[4] R. van Roij, M. Dijkstra, and R. Evans, Europhys. Lett. **49**, 350 (2000); M. Dijkstra, R. van Roij, and R. Evans, Phys.Rev. E **63**, 051703 (2001)
[5] L. Harnau, and S. Dietrich, Phys. Rev. E **66**, 051702 (2002).
[6] I. Rodriguez-Ponce, J. M. Romero-Enrique, E. Velasco, L. Mederos, and L. F. Rull, J. Phys.: Condens. Matter **12**, A363 (2000); I. Rodriguez-Ponce, J. M. Romero-Enrique, and L. F. Rull, Phys. Rev. E **64**, 051704 (2001)
[7] R. E. Webster, N. J. Mottram, and D. J. Cleaver, Phys. Rev. E. **68**, 021706 (2003); Z. Kutnjak, S. Kralj, G. Lahajnar, and S. Zumer, Phys. Rev. E **70**, 051703 (2004).
[8] D. de las Heras, E. Velasco, and L. Mederos, Phys. Rev. Lett. **94**, 017801 (2005); Phys. Rev. E **74**, 011709 (2006).
[9] V. M. Kaganer, H. Mohwald, and P. Dutta, Rev. Mod. Phys. **71**, 779 (1999).
[10] I. S. Aranson, and L. S. Tsimring, Rev. Mod. Phys. **78**, 641 (2006).
[11] P. M. Reis, R. A. Ingale, and M. D. Shattuck, Phys. Rev. Lett. **96**, 258001 (2006).
[12] V. Narayan, N. Menon, and S. Ramaswamy, J. Stat. Mech. P01005 (2006)
[13] Y. Martínez-Ratón, E. Velasco, and L. Mederos, J. Chem. Phys. **122**, 064903 (2005); J. Chem. Phys. **125**, 014501 (2006).
[14] A. Donev, J. Burton, F. H. Stillinger, and S. Torquato, Phys. Rev. B **73**, 054109 (2006).
[15] A. Fierro, M. Nicodemi, and A. Coniglio, Eurphys. Lett. **59**, 642 (2002); Phys. Rev. E **66**, 061301 (2002); A. Coniglio, A. Fierro, and N. Nicodemi, Eur. Phys. J. E **9**, 219 (2002).
[16] D. S. Dean, and A. Lefevre, Phys. Rev. Lett **90**, 198301 (2003).
[17] J. Galanis, D. Harries, and D. L. Sackket, Phys. Rev. Lett. **96**, 028002 (2006).
[18] D. Chaudhuri, and S. Sengupta, Phys. Rev. Lett. **93**, 115702 (2004).
[19] Y. Rosenfeld, M. Schmidt, H. Löwen, and P. Tarazona, J. Phys.: Condens. Matt. **8**, L577 (1996); Phys. Rev. E **55**, 4245 (1997); P. Tarazona, and Y. Rosenfeld, Phys. Rev. E **55**, R4873 (1997).
[20] J. A. Cuesta and Y. Martínez–Ratón, Phys. Rev. Lett. **78**, 3681 (1997); J. Chem. Phys. **107**, 6379 (1997).
[21] R. van Roij, P. Bolhuis, B. Mulder, and D. Frenkel, Phys. Rev. E **52**, R1277 (1995).
[22] J. S. van Duijneveldt, and M. P. Allen, Molec. Phys. **90**, 243 (1997).
[23] Y. Martínez-Ratón, Phys. Rev. E **69**, 061712 (2004).
[24] R. Lipowsky, J. Appl. Phys. **55**, 2485 (1984).
[25] A. Poniewierski, and R. Holyst, Phys. Rev. A **38**, 3721 (1988).
[26] A. Chrzanowska, P. I. C. Teixeira, H. Ehrentraut, and D. J. Cleaver, J. Phys.: Condens. Matter **13**, 4715 (2001).
[27] Y. Martínez-Ratón, A. M. Somoza, L. Mederos, and D. E. Sullivan, Faraday Discuss. **104**, 111 (1996); Y. Martinez, A. M. Somoza, L. Mederos, and D. E. Sullivan, Phys. Rev. E **53** 2466 (1996).
[28] T. J. Sluckin and A. Poniewierski, Molec. Cryst. Liq. Cryst. **179**, 349 (1990).